Vacuum-UV negative photoion spectroscopy of CH3F, CH3Cl and CH3Br

Rogers, Nicola J.; Simpson, Matthew J.; Tuckett, Richard P.; Dunn, Ken F.; Latimer, CJ

DOI:
10.1039/c0cp00234h

Vacuum-UV negative photoion spectroscopy of CH_3F, CH_3Cl and CH_3Br

Nicola J. Rogers,[a] Matthew J. Simpson,[a] Richard P. Tuckett,*[a] Ken F. Dunn[b] and Colin J. Latimer[b]

Received 15th April 2010, Accepted 14th June 2010
DOI: 10.1039/c0cp00234h

Using tunable vacuum-UV radiation from a synchrotron, negative ions are detected by quadrupolar mass spectrometry following photoexcitation of three gaseous halogenated methanes CH_3X (X = F, Cl, Br). The anions X^-, H^-, CX^-, CHX^- and CH_2X^- are observed, and their ion yields recorded in the range 8–35 eV. The anions show a linear dependence of signal with pressure, showing that they arise from unimolecular ion-pair dissociation, generically described as $AB + h\nu \rightarrow A^- + B^+$ (+ neutrals). Absolute cross sections for ion-pair formation are obtained by calibrating the signal intensities with those of F^- from both SF_6 and CF_4. The cross sections for formation of $X^- + CH_3^+$ are much greater than for formation of $CH_2X^- + H^+$. In common with many quadrupoles, the spectra of m/z 1 (H^-) anions show contributions from all anions, and only for CH_3Br is it possible to perform the necessary subtraction to obtain the true H^- spectrum. The anion cross sections are normalised to vacuum-UV absorption cross sections to obtain quantum yields for their production. The appearance energies of X^- and CH_2X^- are used to calculate upper limits to 298 K bond dissociation energies for $D^o(H_3C–X)$ and $D^o(XH_2C–H)$ which are consistent with literature values. The spectra suggest that most of the anions are formed indirectly by crossing of Rydberg states of the parent molecule onto an ion-pair continuum. The one exception is the lowest-energy peak of F^- from CH_3F at 13.4 eV, where its width and lack of structure suggest it may correspond to a direct ion-pair transition.

1. Introduction

Ion-pair formation from an isolated gas-phase polyatomic molecule is a unimolecular dissociative process in which an anion–cation pair is formed following photoexcitation, *i.e.* $AB + h\nu \rightarrow A^- + B^+$ (+ neutrals). Vacuum-UV photons with energy in excess of *ca.* 10 eV are typically needed. Ion-pair production can either occur directly into the ion-pair continuum, or indirectly following predissociation of an initially-excited Rydberg state into the continuum. In both cases, the appearance energy of the anion A^-, $AE(A^-)$, is constrained to the following energetics:

$$AE(A^-) \geq D^o(A–B) + IE(B) - EA(A) \qquad (I)$$

where D^o is a dissociation energy, IE an ionisation energy and EA an electron affinity. On Franck–Condon grounds the latter process of predissociation is more common,[1] so the detection of ion pairs provides information on the electronic structure of a molecule and the decay dynamics of its excited states. An alternative way to express the inequality of eqn (I) is to write[2]

$$AE(A^-) \geq IE(AB) + D^o(A–B^+) - EA(A) \qquad (II)$$

For the three titled molecules, the threshold for ion-pair formation lies below that of molecular photoionisation since the electron affinity of the halogen atom X (X = F, Cl or Br) exceeds $D^o(CH_3X^+ \rightarrow CH_3^+ + X)$. Detection of anions therefore at low energies is relatively facile because there is no overlapping electron signal.

Our interest in the CH_3X series of halo-substituted methanes, where X = F, Cl or Br, is primarily fundamental—to compare data and see the trends in changing the substituent X. CH_3Cl and CH_3Br are anthropogenic sources of Cl and Br atoms in the marine boundary layer.[3] Although nearly all solar VUV radiation is absorbed in the mesosphere, it is important to understand the effects of VUV radiation interacting with these important constituents of the earth's atmosphere. CH_3I was not studied because previous work has shown that the cross sections are too small to produce measurable quantities of ion pairs in the VUV region.[1]

All three CH_3X molecules studied have C_{3v} symmetry, and the main effect of changing X is to lengthen and subsequently weaken the C–X bond. The valence molecular orbitals can be labelled $\ldots(2a_1)^2(1e)^4(3a_1)^2(2e)$,[4] where the 2e orbital is essentially non-bonding X npπ orbitals and the three lower orbitals arise from the σ-bonding framework formed from overlap of the C 2s (a_1), C 2p (a_1 + e) with 3H (a_1 + e) and X np (a_1) atomic orbitals. For CH_3Cl and CH_3Br, the 3p/4p π-orbitals of Cl/Br show little mixing with the CH_3X σ-orbitals where the evidence is best provided from HeI, HeII or threshold photoelectron spectroscopy.[4–7] Both molecules show the effects of

[a] *School of Chemistry, University of Birmingham, Edgbaston, Birmingham B15 2TT, UK. E-mail: r.p.tuckett@bham.ac.uk; Fax: +44 (0)121 414 4403; Tel: +44 (0)121 414 4425*
[b] *Department of Physics and Astronomy, Queen's University Belfast, Belfast BT7 1NN, UK*

spin–orbit splitting, but limited vibrational structure in the $(2e)^{-1}$ first band with a strong $\nu^+ = 0$ transition, showing that the electron has been removed from an orbital that is essentially non-bonding in character. By contrast, the first photoelectron band of CH_3F shows no measurable spin–orbit splitting, but an extended vibrational progression.[4] Indeed, molecular orbital calculations show that the 2e orbital in this molecule has a degree of anti-bonding character, probably due to the ability of the fluorine 2pπ atomic orbitals to interact with other orbitals of equivalent symmetry, inducing secondary mixing. This effect is not observed with CH_3Cl and CH_3Br because pπ-bonding is dependent on internuclear distance. Electron removal from the lower-energy $3a_1$, 1e and $2a_1$ valence orbitals of CH_3F, CH_3Cl and CH_3Br shows very similar features in the photoelectron spectra, as these orbitals are based on the CH_3 σ-bonding framework with only the $3a_1$ orbital showing a minor contribution from the X np orbitals. The ionisation energies of the $(3a_1)^{-1}$ and $(1e)^{-1}$ bands in CH_3F are close together, and it has been speculated that their order might be reversed, relative to the equivalent bands in the heavier halides.[8,9]

In this paper, we report the formation of anions from CH_3X following photoexcitation with tunable VUV radiation in the range 10–35 eV from a synchrotron. An earlier study by Suzuki *et al.* observed the X^- anion from these molecules, and cross sections of anion formation were estimated to be between 10^{-21} and 10^{-20} cm^2.[10] We extend this work and report the formation of X^-, H^-, CH_2X^- and CHX^-. Apart from H^-, absolute cross sections for formation of all anions are also reported. Our work also extends that of Shaw *et al.* on CH_3Cl and CH_3Br where the use of a double ion chamber with no mass selection meant that the identity of the ions produced was not known.[2] Ion-pair imaging studies have been performed following laser photoexcitation at *ca.* 10.5 eV for CH_3Cl and CH_3Br, looking at the CH_3^+/X^- pair.[11–13] Anisotropy in the ion distributions was observed, and analysed to gain information on the dissociation dynamics of the initially-excited Rydberg state. Ion-pair dissociation from $CH_3F \rightarrow CH_3^+ + F^-$ has also been studied by imaging techniques at the higher energy of 21.3 eV.[14] Finally, we note that high-resolution absorption studies have recently been performed on CH_3F, CH_3Cl and CH_3Br by Locht *et al.*,[15–17] and since most anion formation is attributed to the predissociation of Rydberg states these studies are useful for comparison.

2. Experimental and procedure

The ion-pair apparatus has been described in detail elsewhere.[18] Briefly, an effusive jet of the gas under investigation is injected from a needle and intersects orthogonally the incident photon beam. The crossing point is positioned between two grids along the third orthogonal axis. A potential difference applied across these grids attracts negative ions towards a three-element electrostatic lens for focussing, and into a Hiden Analytical HAL IV triple quadrupole mass spectrometer (QMS) for mass selection and detection by a channeltron electron multiplier. The apparatus and QMS are connected *via* a 1 mm diameter aperture, and pumped by separate turbomolecular pumps which are backed by a common rotary pump. Differential pumping enhances sensitivity by reducing the number of free electrons and secondary collisions in the QMS. Tunable radiation in the range 10–35 eV was provided by beamline 3.1 (equipped with a 1 m focal length Wadsworth monochromator) from the UK Daresbury Synchrotron Radiation Source.[19] Two gratings, mounted back-to-back in the monochromator, cover this range of energies, although the majority of these studies used the higher-energy grating ($h\nu > 12$ eV). The optimum resolution of the beamline is 0.05 nm, corresponding to *ca.* 0.01 eV at 15 eV. However, to enhance sensitivity, the spectra reported in this paper were recorded at a degraded resolution. A capillary light guide connects the beamline to the experimental apparatus, providing the necessary differential pumping.

The base pressure of the apparatus was *ca.* 10^{-7} mbar. The pressure was measured in the main chamber using an ionisation gauge, and the introduction of the sample gas to the system raised the pressure to *ca.* 10^{-5} mbar. The sensitivity of the ionisation gauge to CH_3X (X = F, Cl, Br), SF_6 and CF_4, which is essential for determination of *absolute* cross sections of anion formation, was calibrated in a separate experiment relative to N_2 using a capacitance manometer.[20] Gas samples were supplied by Apollo Scientific or Aldrich Chemical Company, and were used without further purification.

Following exposure to white light with the grating set to zero order, mass spectra were recorded to observe all the anions produced by photoabsorption of the sample gas. The mass-to-charge ratio (m/z) of each peak in the mass spectrum was then defined, and the ion yield recorded as a function of photon energy. Once the peak positions were determined, the anion signal was recorded as a function of gas pressure over a typical range of *ca.* $(0.5–5.0) \times 10^{-5}$ mbar. Anions displaying a linear dependence with pressure can be attributed to ion-pair formation, defined in Section 1, whereas those showing a non-linear pressure dependence cannot. The latter are likely to result from the two-step kinetic process of dissociative electron attachment (*i.e.* $AB + h\nu \rightarrow AB^+ + e^-$; $AB + e^- \rightarrow A^- + B$), in which the rate of formation of A^- is proportional to the square of the pressure of AB.[21] With the exception of $CHBr^-$ from CH_3Br in which time constraints at the beamline precluded the measurement, the signals of all anions observed from CH_3F, CH_3Cl and CH_3Br showed a linear dependence with pressure. Since the CHF^-/CH_3F signal is first order with respect to pressure, we have analysed the $CHBr^-/CH_3Br$ signal assuming that it is also formed by ion-pair formation.

To determine absolute cross sections of the anions from ion-pair formation, the anion signal must be normalised to the photon flux, the ring current, the gas pressure, the ionisation gauge sensitivity, and the relative mass sensitivity of the QMS to detection of the different anions. As in our previous studies on SF_5CF_3,[21] the CF_3X series (X = Cl, Br, I),[22] and CH_4,[23] we can write that:

$$\sigma(h\nu) = k\left(\frac{SM}{frpI}\right) \qquad \text{(III)}$$

where S is the detected signal normalised to unit time, f is the relative photon flux which effectively is a measure of the

grating efficiency, r is the storage ring current, p is the sample gas pressure corrected for ionisation gauge sensitivity (see above), I is the isotope correction factor which is only pertinent for anions containing one Cl or Br atom, and M is the relative mass sensitivity of the QMS. k is the constant of normalisation. In detecting chlorine-containing anions from CH_3Cl, only the ^{35}Cl isotopomer was detected. Likewise, for bromine-containing anions from CH_3Br, only the ^{79}Br isotopomer was detected. Therefore, for these anions I takes the value 0.758 and 0.507 to account for the experiment only detecting 75.8% and 50.7%, respectively, of the true signal. Normalisation to I, but also to f, r and p, is therefore facile, but the process is slightly more complicated for M. An extensive set of experiments was performed to determine M as a function of (m/z), described elsewhere.[23] As m/z increases, the detection efficiency of the QMS decreases, and a higher value of M is needed to correct this effect; thus, M rises from 0.27 for m/z 19 (F^-) non-linearly to 1.86 for m/z 93 ($CH_2{}^{35}Br^-$, the heaviest anion detected), with m/z 69 ($CF_3{}^-$) arbitrarily being given the value $M = 1$. Finally, the zero-blast artefact,[24] whereby *all* ions entering the quadrupole mass filter may be transmitted when the applied potentials are set to detect m/z 1 (*i.e.* H^-), is an important factor in this study because H^- from all three CH_3X molecules, whilst observed in all cases, is not the dominant anion. The H^- yield from CH_3X therefore appears on top of a background scan that mimics that of X^-, the dominant anion. To determine the true H^- yield, it was necessary to subtract a scaled X^- spectrum from the normalised H^- spectrum. The determination of an absolute cross section for H^- production was therefore not possible. This is different from the formation of H^- from CH_4 where this anion is dominant, so an absolute value for σ can be determined.[23]

The normalised signals are then put onto an absolute scale by determining the F^- signal strengths in our experiment from SF_6 and CF_4, and calibrating them to values of the cross section determined by Mitsuke *et al.* for SF_6 ($(7 \pm 2) \times 10^{-21}$ cm^2 at 14.3 eV)[25] and CF_4 ($(1.25 \pm 0.25) \times 10^{-21}$ cm^2 at 13.9 eV).[26] (We note that these cross sections are not strictly absolute, but obtained indirectly from the signal of O^- produced from O_2 at 17.3 eV for which the absolute cross section is known.[27] Future experiments will probably calibrate the signals directly with O^- from O_2.) The values of the normalisation constants, k (F^-/SF_6) and k (F^-/CF_4), should be equivalent, but in fact they differ by a factor of *ca.* 1.5. Given the number of corrections made to the anion signals in the two experiments, this discrepancy falls within a reasonable expected experimental uncertainty. The average value of k was then used in eqn (1) to determine the absolute cross sections, σ, in units of cm^2, for production of X^-, CH_2X^- and CHX^- from CH_3X. We estimate that these cross sections are accurate to a factor of *ca.* 2. Due to the zero-blast artefact, only the relative cross sections for production of H^- from CH_3X are reported (see earlier).

3. Thermochemistry

Our work determines appearance energies at 298 K (AE_{298}) for fragment anions from CH_3F, CH_3Cl and CH_3Br, and they are compared with calculated thermochemical values. Berkowitz noted that for many polyatomic molecules, when suitable assumptions are made about the nature of the accompanying cation and neutral fragment(s), a calculated threshold energy is a lower limit to the experimental AE_{298} of an anion.[1] Furthermore, in comparing experimental AE_{298} values of anions with calculated enthalpies of appropriate dissociation reactions, $\Delta_rH^o{}_{298}$, we are making two assumptions which are justified at the relatively modest resolution of the experiment, *ca.* 0.1–0.2 eV. First, although it is not accurate to equate an AE_{298} to $\Delta_rH^o{}_{298}$ because of thermal effects,[28] however the corrections needed to the AE_{298} values are typically only 0.05–0.15 eV, and we feel justified in ignoring them. Second, the effects of entropy are disregarded, even though all unimolecular reactions involve $\Delta n > 0$, where Δn is the stoichiometric number of product species minus the number of reactant species. Thus $\Delta_rS^o{}_{298}$ will be positive, and $\Delta_rG^o{}_{298}$ for the unimolecular reactions will be more negative than the calculated $\Delta_rH^o{}_{298}$ values.

Values for $\Delta_rH^o{}_{298}$ of relevant ion-pair reactions were calculated using literature values for enthalpies of formation ($\Delta_fH^o{}_{298}$ in kJ mol^{-1}): $CH_3F = -234.3$, $CH_3Cl = -83.7$, $CH_3Br = -34.3$; $CH_2F^- = -53$, $CH_2Cl^- = 45$, $CH_2Br^- = 75$; $CHF^- = 109$, $CHBr^- = 231$; $CF^- = -63$; $F^- = -249$, $Cl^- = -227$, $Br^- = -213$; $H^- = 145$; $H^+ = 1530$, $H_2{}^+ = 1488$; $CH_3{}^+ = 1098$.[29,30]

4. Results

4.1 CH_3F

The ion yields and absolute cross sections for formation of F^-, CF^-, CHF^- and CH_2F^- from CH_3F in the range 12–35 eV are shown in Fig. 1(a)–(d), respectively. The data are collected in Table 1. The spectra were recorded on the high-energy grating with a resolution of 0.6 nm, corresponding to 0.07 eV at 12 eV and 0.28 eV at 24 eV. The F^- signal is the most intense. Scans at m/z 1 and 15 (H^- and $CH_3{}^-$) both mimic the F^- spectrum,

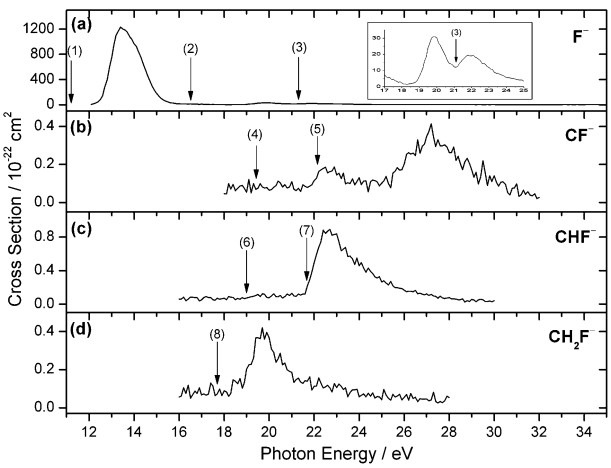

Fig. 1 Absolute cross sections for F^-, CF^-, CHF^- and CH_2F^- (a–d) production following vacuum-UV photoexcitation of CH_3F. Ion yields were measured between 12 and 32 eV at a wavelength resolution of 0.6 nm. Solid arrows show the energies of the thermochemical thresholds calculated for reactions (1)–(8) (Section 4.1).

Table 1 Appearance energies, cross sections and quantum yields for anions observed from photoexcitation of CH_3F, CH_3Cl and CH_3Br

Molecule	Anion	AE_{298}/eV	Cross section/cm^2	Energy of cross section maximum/eV	Quantum yield[h]
CH_3F	F^-	12.28 ± 0.02[a]	1.2×10^{-19}	13.4	2.3×10^{-3}
CH_3F	CF^-	24.4 ± 0.2[b,c]	4.2×10^{-23}	27.2	1.5×10^{-6}
CH_3F	CHF^-	21.5 ± 0.2[b]	8.8×10^{-23}	22.4	2.2×10^{-6}
CH_3F	CH_2F^-	18.2 ± 0.2[b]	4.1×10^{-23}	19.7	8.9×10^{-7}
CH_3Cl	Cl^-	10.04 ± 0.02[a]	1.2×10^{-19}	11.3	2.3×10^{-3}
CH_3Cl	CH_2Cl^-	17.2 ± 0.2[b]	7.6×10^{-21}	18.2	1.0×10^{-4}
CH_3Br	H^-	12.1 ± 0.2[d]	—[f]	14.0	—
CH_3Br	Br^-	9.46 ± 0.02[a]	2.5×10^{-20}	10.0	4.1×10^{-4}
CH_3Br	$CHBr^-$	*ca.* 20[e]	1.3×10^{-22}[g]	22.4	3.3×10^{-6}
CH_3Br	CH_2Br^-	17.1 ± 0.2[b]	5.6×10^{-22}	17.8	8.1×10^{-6}

[a] Appearance energy (AE) observed from this work, from the high resolution spectra shown in Fig. 4. [b] Appearance energy (AE) observed from this work, from the spectra shown in Fig. 1–3. [c] The AE(F^-) given here assumes that the peak at 22.5 eV in Fig. 1(b) is an overlap of CHF^- signal. [d] AE is difficult to determine, as scan starts as 12 eV and the subtraction method discussed in Section 2 has been implemented. [e] Cannot determine AE with confidence due to poor signal to noise. The signal may have contributions from CH_2Br^-. [f] Cross section cannot be determined due to the zero-blast effect, discussed in Section 2. [g] Cross sections are determined for the $CHBr^-$ anion, assuming that its signal varies linearly with pressure. [h] Quantum yields for anion production are obtained by dividing cross sections for anion production (column 4) by the total absorption cross sections. The latter values are taken from data for CH_3F, CH_3Cl and CH_3Br respectively.[15–17,34]

but are artefacts for different reasons. The H^- normalised signal, whilst being only *ca.* 10% of the normalised F^- signal, has an identical relative ion yield to that of F^- over the range 12–16 eV due to the zero-blast effect, the contribution of all anions to the m/z 1 signal in many quadrupole mass spectrometers.[24] A subtracted spectrum could therefore not be trusted. The CH_3^- signal at m/z 15 is too close in mass to the very strong m/z 19 signal, and thus any CH_3^- signal lies in the tail of the much stronger F^- signal. The same problem inhibited possible detection of HF^- (m/z 20). There is no similarity between any of the four anion yields and the photoelectron spectrum of CH_3F over this energy range. For example, the strong F^- signal shows an onset at 12.28 ± 0.02 eV and a maximum at 13.4 eV, whilst the first photoelectron band has adiabatic and vertical ionisation energies of 12.53 and 13.04 eV, respectively.[4] In addition to the linearity of the anion signal *vs.* pressure tests, these provide evidence that all four anions are not formed by dissociative electron attachment but by ion-pair dissociation.

The arrows in Fig. 1 show the calculated $\Delta_r H^\circ_{298}$ values for possible ion-pair dissociation reactions (1)–(8). As described earlier, we do not distinguish a reaction *enthalpy* from a reaction *energy* at the relatively low resolution of this experiment. They take the values 11.18, 16.47, 21.15, 19.46, 22.15, 18.98, 21.67 and 17.73 eV, respectively.

$$CH_3F \rightarrow F^- + CH_3^+ \quad (1)$$

$$CH_3F \rightarrow F^- + CH_2^+ + H \quad (2)$$

$$CH_3F \rightarrow F^- + CH^+ + 2H \quad (3)$$

$$CH_3F \rightarrow CF^- + H_2^+ + H \quad (4)$$

$$CH_3F \rightarrow CF^- + H^+ + 2H \quad (5)$$

$$CH_3F \rightarrow CHF^- + H_2^+ \quad (6)$$

$$CH_3F \rightarrow CHF^- + H^+ + H \quad (7)$$

$$CH_3F \rightarrow CH_2F^- + H^+ \quad (8)$$

4.2 CH_3Cl

The ion yields and absolute cross sections for the formation of Cl^- and CH_2Cl^- from CH_3Cl in the range 8–35 at a resolution of 0.6 nm are shown in Fig. 2(a) and (b), respectively. The spectrum of the strongest anion, Cl^-, was run on both gratings from 8–18 eV (low energy) and 12–35 eV (high energy), and the spectra merged. The CH_2Cl^- spectrum was obtained on the high-energy grating. Only these two anions could conclusively be detected, because resolving m/z values of fragments differing by 1 u is very difficult in chlorine-containing moieties; a spectrum recorded with m/z 48 (*i.e.* $CHCl^-$) was identical to

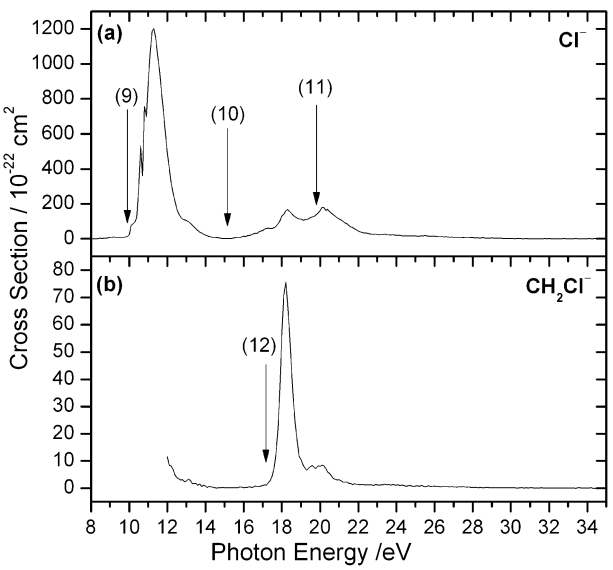

Fig. 2 Absolute cross sections for Cl^- (a) and CH_2Cl^- (b) production following vacuum-UV photoexcitation of CH_3Cl. Ion yields were measured between 8 and 34 eV at a wavelength resolution of 0.6 nm. Solid arrows show the energies of the thermochemical thresholds calculated for reactions (9)–(12) (Section 4.2).

that of m/z 49, but thermochemistry shows that the signal, with a threshold of 17.2 ± 0.2 eV, can only be due to CH_2Cl^- (Section 5.3). An H^- spectrum was recorded, but its shape and resolved features were identical to those of Cl^-, although a factor of *ca.* 40 weaker. A subtracted spectrum, to yield the true H^- spectrum, could not therefore be obtained reliably. An HCl^- spectrum with m/z 36 was recorded, but its mass lies in between the two isotopes of chlorine, so the presence of this anion is deemed uncertain. A spectrum of CH_2Cl^- was also run with the low-energy grating and a LiF window only transmitting $h\nu < 11.8$ eV. No peaks were detected. The apparent rise in the signal of this anion for $h\nu < 14$ eV on the high-energy grating (Fig. 2(b)) is probably an artefact due to inaccurate flux normalisation at these energies, where the flux is low.

The arrows in Fig. 2 show the calculated $\Delta_r H^o_{298}$ values for possible ion-pair dissociation reactions (9)–(12). They take values 9.85, 15.14, 19.85 and 17.19 eV, respectively.

$$CH_3Cl \rightarrow Cl^- + CH_3^+ \quad (9)$$

$$CH_3Cl \rightarrow Cl^- + CH_2^+ + H \quad (10)$$

$$CH_3Cl \rightarrow Cl^- + CH^+ + 2H \quad (11)$$

$$CH_3Cl \rightarrow CH_2Cl^- + H^+ \quad (12)$$

4.3 CH_3Br

The ion yields for formation of H^-, Br^-, $CHBr^-$ and CH_2Br^- from CH_3Br in the range 9–35 eV at a resolution of 0.6 nm are shown in Fig. 3(a)–(d), respectively. As with CH_3Cl, both gratings were needed to record the spectrum of the strongest anion, Br^-, since the threshold energy is observed at 9.46 ± 0.02 eV. The H^- spectrum was also recorded on both gratings. Over the range 9.5–12.0 eV the spectrum was identical to that of Br^-, and it was not possible to obtain a subtracted 'true H^-' spectrum. Above 12 eV on the high-energy grating, however, the Br^- signal is much weaker, the two spectra were significantly different, and it was possible to perform a Br^- subtraction to obtain the true H^- spectrum (Fig. 3(a)). Thus the cross sections in Fig. 3(b)–(d) are accurate to the usual error of a factor of two, but only relative cross sections for production of H^- are shown in Fig. 3(a). For reasons outlined in Section 4.2 above, the very weak $CHBr^-$ spectrum (m/z 92) may contain a component of the CH_2Br^- spectrum (m/z 93). It was analysed, however, assuming that it is a clean m/z 92 signal and, as explained in Section 2, that it is formed by ion-pair dissociation in conjunction with a cation (H_2^+ or H^+).

The arrows in Fig. 3 show the calculated $\Delta_r H^o_{298}$ values for possible ion-pair dissociation reactions (13)–(21). They take values 11.57, 17.38, 22.09, 9.53, 14.77, 19.48, 18.17, 20.86 and 16.99 eV, respectively.

$$CH_3Br \rightarrow H^- + CH_2Br^+ \quad (13)$$

$$CH_3Br \rightarrow H^- + CH_2^+ + Br \quad (14)$$

$$CH_3Br \rightarrow H^- + CH^+ + H + Br \quad (15)$$

$$CH_3Br \rightarrow Br^- + CH_3^+ \quad (16)$$

$$CH_3Br \rightarrow Br^- + CH_2^+ + H \quad (17)$$

$$CH_3Br \rightarrow Br^- + CH^+ + 2H \quad (18)$$

$$CH_3Br \rightarrow CHBr^- + H_2^+ \quad (19)$$

$$CH_3Br \rightarrow CHBr^- + H^+ + H \quad (20)$$

$$CH_3Br \rightarrow CH_2Br^- + H^+ \quad (21)$$

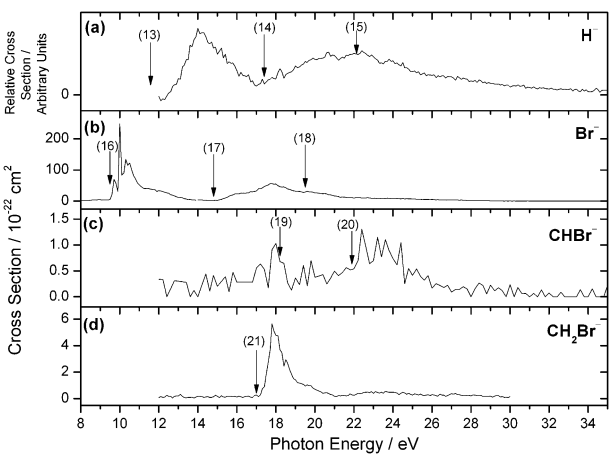

Fig. 3 Relative (H^- (a)) and absolute (Br^-, $CHBr^-$, CH_2Br^- (b–d)) cross sections for anion production following vacuum-UV photoexcitation of CH_3Br. Ion yields were measured between 8 and 34 eV at a wavelength resolution of 0.6 nm. Solid arrows show the energies of the thermochemical thresholds calculated for reactions (13)–(21) (Section 4.3). The cross section for $CHBr^-$ is determined, assuming that this anion is formed by ion-pair dissociation (Sections 2 and 4.3).

4.4 Higher resolution studies

The X^-/CH_3X ion curves for the strong first peak are shown at a higher resolution of 0.2 nm in Fig. 4. The F^- curve shows a gradual onset and no apparent structure at this resolution, with most of the intensity appearing at higher energy than the adiabatic ionisation energy of CH_3F (*i.e.* to the $\tilde{X}\ ^2E$ ground state of CH_3F^+). By contrast, for Cl^- and Br^- much of the signal lies below the energy of the lower spin–orbit resolved $\tilde{X}\ ^2E_{3/2}$ state of CH_3Cl^+ and CH_3Br^+. The spectra, discussed in Section 5, show discrete resolved structure, and they are very similar to photoabsorption spectra of CH_3Cl and CH_3Br over this energy range.[16,17] They correspond to Rydberg states of CH_3Cl or CH_3Br converging on the $\tilde{X}\ ^2E$ state of the parent ion which are crossed by predissociating ion-pair states to form Cl^- or $Br^- + CH_3^+$. The X^-/CH_3X ion curves for the weaker peaks between 16–24 eV are expanded in Fig. 5. Suzuki *et al.* have commented that these peaks lie between the $\tilde{B}\ ^2E$ and $\tilde{C}\ ^2A_1$ states of CH_3X^+, and therefore probably correspond to Rydberg states of CH_3X converging on the $\tilde{C}\ ^2A_1$ state of the ion.[10] As above, they cross with (different) predissociating ion-pair states to form $X^- + CH_3^+$. Their assignments are discussed in Section 5.

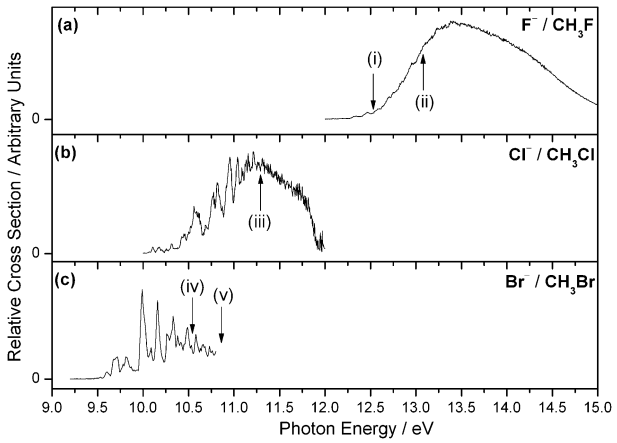

Fig. 4 The threshold region for production of X^- from CH_3X recorded with a step size of 0.005 eV and a wavelength resolution of 0.2 nm, corresponding to *ca.* 0.02 eV at 12 eV. Absolute cross sections are not shown because the calibration signals of F^- from CF_4 and SF_6 were not measured at this resolution. (a) (i) and (ii) show the energies of the adiabatic and vertical ionisation energy of the first photoelectron band of CH_3F.[4] (b) (iii) shows the energy of the adiabatic or vertical ionisation energy of the first band of CH_3Cl, ionisation to CH_3Cl^+ $\tilde{X}\,^2E$ where the spin–orbit splitting is very small, 0.027 eV.[4,7] (c) (iv) and (v) show the energies of the adiabatic ionisation energy of the two spin–orbit components of CH_3Br^+ $\tilde{X}\,^2E_{3/2}$ and $^2E_{1/2}$ where the spin–orbit splitting is much larger, 0.320 eV.[6]

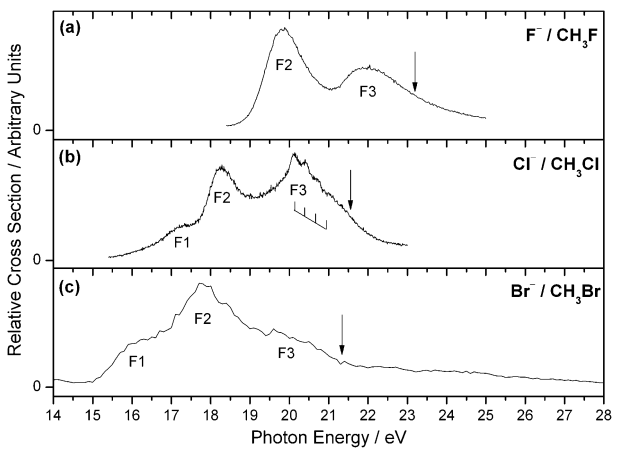

Fig. 5 Relative cross sections for production of X^- from CH_3X between 14 and 28 eV recorded at a resolution of 0.6 nm. Features F1, F2 and F3 are described in the text, and assigned in Table 2. The arrows show the vertical ionisation energies of the fourth photoelectron band, ionisation to $\tilde{C}\,^2A_1$. A progression with approximate spacing of 0.27 eV is observed in F3 of the Cl^-/CH_3Cl spectrum, probably corresponding to vibrational structure in the $(2a_1)^{-1}4s$ Rydberg state of CH_3Cl (see text).

5. Discussion

5.1 X^- from CH_3X at threshold

On thermochemical grounds, the X^- anion can only form with CH_3^+ at the first peak of each X^-/CH_3X spectrum in the 9–15 eV range (see Fig. 1–4). The F^-/CH_3F and Cl^-/CH_3Cl spectra in Fig. 4(a) and (b) correspond well to data published by Suzuki *et al.*,[10] but they could not detect a Br^-/CH_3Br spectrum at low energy due to the poor flux from the monochromator used below 10 eV. Apart from a brief report in the review article by Berkowitz,[1] this is the first detailed observation of Br^- from CH_3Br. We determine AE_{298} values for F^-, Cl^- and Br^- of 12.28 ± 0.02, 10.04 ± 0.02 and 9.46 ± 0.02 eV (Table 1). These values lie below the respective ionisation energies to the $\tilde{X}\,^2E_{3/2}$ state of CH_3X^+ of 12.53, 11.29 and 10.54 eV (see eqn (II)), and exceed the respective thermochemical values for the appearance energy, given by $D^o(CH_3–X)$ + $IE(CH_3)$ − $EA(X)$, of 11.21, 9.85 and 9.52 eV for X = F, Cl and Br. The inequality of eqn (I) is therefore obeyed in all three cases. The F^- yield shows no structure, whereas discrete transitions can be identified in the Cl^- and Br^- yields.

We consider first the structure in CH_3Cl and CH_3Br. As described in Section 1, the ground-state photoelectron band of these molecules, removal of an electron from the 2e HOMO, has only limited vibrational structure, with the strongest transitions occurring to $\nu^+ = 0$.[4,6,7] Thus, electronic transitions in CH_3Cl and CH_3Br from the 2e HOMO to a Rydberg state converging on the $\tilde{X}\,^2E$ state of the parent ion would not be expected to exhibit extensive vibrational progressions, but rather sharp Rydberg peaks. Assuming that ion-pair production is indirect, structured features should therefore be observed in the Cl^- and Br^- yields following crossing of the Rydberg potential surface to an ion-pair surface. This is indeed what is observed. The fine structure is complicated by the number of Rydberg series that are allowed, each converging on two spin–orbit-split ionisation thresholds, $\tilde{X}\,^2E_{3/2}$ and $\tilde{X}\,^2E_{1/2}$. These splittings take values of 27 and 305 meV for CH_3Cl^+ and CH_3Br^+, respectively,[4,6,7] and Suzuki *et al.* have assigned the peaks in the Cl^-/CH_3Cl spectrum to members of s, p and d Rydberg series converging on both ion thresholds.[10] Furthermore, at these energies below the adiabatic IE, in studies of CH_3Cl and CH_3Br by Locht *et al.*, the CH_3^+ ion yield duplicates *exactly* our Cl^- and Br^- yields of Fig. 4(b) and (c).[6,31] This is to be expected, since the ion-pair dissociation reaction $CH_3X \rightarrow CH_3^+ + X^-$ is the only ionic channel that is energetically open. We note, however, that the earlier photoabsorption studies by the same group at a resolution of *ca.* 0.01 eV suggest that there is generally good, but not perfect agreement between the absorption spectrum and the Cl^- or Br^- ion yield spectrum below the ionisation energy of CH_3Cl and CH_3Br,[16,17] suggesting that there are competing dissociation channels such as neutral photodissociation. For CH_3Cl, the Rydberg peak assignments given by Locht *et al.* are in good agreement with those reported by Suzuki *et al.*[10] For CH_3Br, Rydberg assignments, again involving s, p and d Rydberg series, are given by Locht *et al.*[17] Neither set of assignments is repeated here.

By contrast, the ground-state photoelectron band of CH_3F, removal of an electron from the 2e HOMO, has extended vibrational structure.[4] The origin of the F^- signal from CH_3F is more uncertain, as its first maximum just exceeds the adiabatic ionisation energy, and thus cannot correspond to Rydberg states converging on $\nu^+ = 0$ of CH_3F^+ $\tilde{X}\,^2E$. Given the large width of the peak and its lack of structure, it is possible that it corresponds to a *direct* ion-pair transition.

Alternatively, Suzuki *et al.* have suggested that this peak consists of unresolved Rydberg states converging to a number of vibrationally-excited levels of CH_3F^+ $\tilde{X}\ ^2E$.[10]

5.2 X^- from CH_3X between 16–24 eV

The peaks observed in all the X^-/CH_3X scans between 16 and 24 eV are shown on an expanded scale in Fig. 5. These peaks all lie between the $\tilde{B}\ ^2E$ and $\tilde{C}\ ^2A_1$ ionisation thresholds of CH_3X^+; the vertical IE for the $\tilde{B}\ ^2E$ ($\tilde{C}\ ^2A_1$) state of CH_3F^+, CH_3Cl^+ and CH_3Br^+ is 17.2 (23.2),[4,5] 16.0 (21.56),[4,7] and 15.0 (21.3) eV,[5,6] respectively. Two peaks are observed in the F^-/CH_3F spectrum (labelled F2 and F3) and three peaks are present in both the Cl^-/CH_3Cl and Br^-/CH_3Br spectra (labelled F1, F2 and F3). Suzuki *et al.* have assigned most of these peaks to Rydberg states of CH_3X converging on the $\tilde{C}\ ^2A_1$ state of the ion,[10] using the well-established Rydberg formula for the energy levels, E_n, of Rydberg series,

$$E_n = \mathrm{IE} - \frac{R_\mathrm{H}}{(n-\delta)^2} \qquad \text{(IV)}$$

The quantum defect, δ, and assignment of the peaks are given in Table 2. Two points should be noted. First, there has been inconsistency in the literature regarding the use of the adiabatic or vertical IE in such calculations, and this choice can significantly affect the Rydberg assignments for high values of n, near the convergence limit. In spectra that consist of many unresolved vibrational modes such as here, it is more appropriate to use the vertical IE because, assuming little change in geometry between Rydberg state and cation, both the vertical Rydberg and vertical ionisation transitions will occur from $\nu'' = 0$ of CH_3X $\tilde{X}\ ^1A_1$ to the same value of ν'. Second, difficulties can arise in comparing Rydberg assignments because different choices in Rydberg-state nomenclature exist. Suzuki *et al.* treat the MOs as an extension of halogen atomic orbitals (AO), with $n = 3/4/5$ for the lowest *n*s and *n*p Rydberg orbitals of $CH_3F/Cl/Br$, respectively.[10] Alternatively, an extension of the carbon AOs can be considered, which is our chosen nomenclature. This renders $n = 3$ for the lowest *n*s and *n*p Rydberg orbitals of all three methyl halides. We believe this to be particularly useful as it emphasises that $(n - \delta)$ is approximately equal for corresponding Rydberg transitions in a series of related molecules, *i.e.* CH_3X.[32] A further reason to choose this nomenclature lies with the nature of the Rydberg electron, which is being removed from the $2a_1$ MO. This MO is based on C–H σ bonds,[4–6,8] and it seems more sensible to use carbon-type Rydberg labels. The quantum defects we determine should then be comparable to those values for atomic C; $\delta = 0.98$ (s), 0.58 (p), 0.01 (d), 0.00 (f).[33] The assignments of Suzuki *et al.* give quantum defects that are more comparable to values for the atomic halogen atom in question. Unassignable n^* values for the F1 transition in CH_3Cl and CH_3Br have been attributed to valence states both by us and by Suzuki *et al.* (Table 1). Finally, we should note that assignments of isolated term values are not conclusive, as different but sensible values of n and δ could correspond to a particular value of E_n. Detailed Rydberg assignments can only be made unambiguously by fitting a whole series of states to the Rydberg formula, usually from absorption spectra.

Table 2 Energies, assignments and quantum defects of the X^-/CH_3X peaks between 16 and 24 eV converging on the $\tilde{C}\ ^2A_1$ state of CH_3X^+

Peak[a]	E_n[b]/eV	Term value[c]/eV	n^*[d,f]	δ[e,f]	Rydberg state
CH_3F (F2)	19.9	3.3[g]	2.03	0.97	3s
			[1.97]	*[1.03]*	*[3s]*
CH_3F (F3)	22.0	1.2[g]	3.37	0.63	4p
			[3.24]	*[−0.24]*	*[3d]*
CH_3Cl (F1)	17.3	4.3[h]	1.78	—	σ*
CH_3Cl (F2)	18.3	3.3[h]	2.03	0.97	3s
			[2.03]	*[1.97]*	*[4s]*
CH_3Cl (F3)	20.1	1.5[h]	3.01	0.99	4s
			[3.24]	*[−0.24]*	*[3d]*
CH_3Br (F1)	16.2	5.1[i]	1.63	—	σ*
CH_3Br (F2)	17.7	3.6[i]	1.94	1.06	3s
			[1.92]	*[3.08]*	*[5s]*
CH_3Br (F3)	19.6	1.7[i]	2.83	0.17	3d
			[2.92]	*[1.08]*	*[4d]*

[a] Peaks displayed in the ion-pair spectrum of the X^-/CH_3X spectrum shown in Fig. 5. [b] E_n is the peak energy of the Rydberg state. [c] Term value is the ionisation energy to which the Rydberg state converges minus the energy of the Rydberg state. [d] n^* is the effective principle quantum number, *i.e.* $(n - \delta)$. [e] δ is the quantum defect. [f] Alternative assignments and data from Suzuki *et al.* are shown in squared brackets.[10] [g] Calculated using the VIE to $\tilde{C}\ ^2A_1$ state of CH_3F^+ of 23.2 eV.[5] [h] Calculated using the VIE to $\tilde{C}\ ^2A_1$ state of CH_3Cl^+ of 21.56 eV.[7] [i] Calculated using the VIE to $\tilde{C}\ ^2A_1$ state of CH_3Br^+ of 21.3 eV.[5]

We note the broad nature of all the peaks in Fig. 5 for production of X^-/CH_3X above *ca.* 16 eV. Furthermore, feature F3 of the Cl^-/CH_3Cl spectrum at 20 eV, assigned to the $(2a_1)^{-1}4s$ Rydberg state, has partially-resolved structure, with 'peaks' observed at 20.13, 20.39, 20.66 and 20.93 eV. This structure was first observed in absorption by Wu *et al.*,[34] and the spacing of *ca.* 0.27 eV or 2180 cm^{-1} is most likely to be vibrational structure in the totally symmetric ν_1 (a_1) mode, since the fourth photoelectron band at 21.56 eV, ionisation to CH_3Cl^+ $\tilde{C}\ ^2A_1$, also shows discrete vibrational structure with peaks at 21.56, 21.83 and 22.09 eV yielding the same vibrational spacing.[7] This reduced value from the ν_1 frequency of 2966 cm^{-1} in the ground state of CH_3Cl is consistent with the $2a_1$ molecular orbital having strong C–H σ-bonding character. Locht *et al.* also observe partially resolved peaks in the $\tilde{C}$-state photoelectron band, with peaks at 21.60, 21.82, 21.98 and 22.14 eV.[31]

In order to explain the linear response of X^- signal with pressure, X^- must form with a cation (+ neutral(s)). It is possible that X^- forms with CH_3^+, just like the X^- signal formed near threshold at *ca.* 10 eV (Section 5.1). However, since the thresholds for Cl^- and Br^- signal in this energy region correspond closely to the enthalpies of reactions (10) and (17) (see Fig. 2(a) and 3(b), respectively), it seems likely that X^- is formed with $CH_2^+ + H$. The enthalpy of reaction (2) is also not inconsistent with this interpretation for F^-/CH_3F. In all three halide molecules, the highest-energy peak, F3, for X^- production has its maximum at an energy slightly above the enthalpy of reactions (3), (11) and (18) for F^-, Cl^- and Br^-, respectively. It is possible, therefore, that

these Rydberg states of CF_3X are crossed by ion-pair surfaces which dissociate to $X^- + CH^+ + 2H$. A coincidence experiment between mass-selected anions and cations, similar to that reported for $CO_2 + h\nu \rightarrow O^- + CO^+$, is needed to take this interpretation further.[35]

5.3 H^-, CH_2X^-, CHX^- and CX^- from CH_3X

As explained in Sections 4.1–4.3, due to the zero-blast effect the H^- yield from CH_3Br (Fig. 3(a)) was the only one of the three H^- spectra where an 'X^--subtracted' spectrum was reliable and genuine. The experimental onset for H^-/CH_3Br of 12.1 ± 0.2 eV, leading to the first peak at 14.0 eV, is compatible with a calculated enthalpy for reaction (13), production of H^- with CH_2Br^+, of 11.57 eV. A second peak at 20.5 eV with a threshold at *ca.* 17 eV is compatible with formation of H^- with $CH_2^+ + Br$ (reaction (14)), calculated threshold 17.38 eV. If there is a third peak present at 23 eV, it correlates reasonably well with the calculated threshold for reaction (15), production of H^- with $CH^+ + H + Br$. The observation of H^- experimental thresholds close to the calculated thresholds for reactions (13)–(15) suggests that H^- forms either with CH_2Br^+ or with fragments of CH_2Br^+ that do not involve the formation of a new bond.

The anions CH_2X^- (X = F, Cl, Br) can only form in an ion-pair reaction in combination with H^+. The appearance energies of these three ions are 18.2 ± 0.2, 17.2 ± 0.2 and 17.1 ± 0.2 eV (Table 1), respectively, in excellent agreement with the enthalpies for reactions (8), (12) and (21) of 17.73, 17.19 and 16.99 eV. Thus, these ions are being formed at threshold, as would be expected in the absence of an exit-channel barrier. The cross sections for forming $CH_2X^- + H^+$ are *ca.* two to four orders of magnitude smaller than for formation of $X^- + CH_3^+$ (Table 1 and Fig. 1–3), the difference being the greatest where X = F. This observation indicates that there is preferential C–X bond cleavage over C–H cleavage for all three molecules. This effect is presumably due to the greater electronegativity value of the fluorine atom compared to the other halogen atoms, polarising significantly the $C^{\delta+}$–$F^{\delta-}$ bond in the neutral molecule. The C–H bonds in all three molecules are much less polarised, making formation of $CH_2X^- + H^+$ a weaker process with lower cross section.

The CHF^- and $CHBr^-$ anions show experimental thresholds at 21.5 and *ca.* 20 eV, respectively, although the spectrum of the latter anions shows a poor signal-to-noise ratio. These thresholds compare reasonably with calculated enthalpies of reactions (7) and (20) of 21.67 and 20.86 eV, suggesting that the accompanying products are probably $H^+ + H$, and not H_2^+. As explained earlier, the ion yield of $CHCl^-$ could not be determined with certainty due to mass resolution effects. The CF^- spectrum (Fig. 1(b)) shows a weak peak at 22.5 eV with an onset of 21.4 eV. The latter energy slightly precedes the thermochemical onset of reaction (5), 22.1 eV. This part of the CF^- signal is therefore more likely to result from the overlap of signal from CHF^- (Fig. 1(c)), and the true AE(CF^-) is deemed to be at the higher energy of 24.4 ± 0.2 eV. The cross sections for production of CCl^- and CBr^- were too weak for the yields of these anions to be measured.

The peaks in all the X^-/CH_3X spectra from 16–24 eV have been assigned to predissociating Rydberg states converging on the $\tilde{C}\ ^2A_1$ state of CH_3X^+ which dissociate into ion-pair continua (Section 5.2). We note that feature F2 of Fig. 5 of the F^-/CH_3F spectrum occurs at the same energy, *ca.* 19.8 eV, as the peak in the CH_2F^- spectrum (Fig. 1). This suggests that both the $F^- + CH_3^+$ and $CH_2F^- + H^+$ ion-pair states cross the $(2a_1)^{-1}3s$ Rydberg states of CH_3F, and the different intensities of the two peaks reflect the different coupling of the ion-pair states to this particular Rydberg state. Similarly, features F2 and F3 of the Cl^-/CH_3Cl spectrum of Fig. 5 at 18.2 and 20.1 eV match the positions of both peaks in the CH_2Cl^-/CH_3Cl spectrum (Fig. 2), and feature F2 of the Br^-/CH_3Br spectrum of Fig. 5 has approximately the same energy, 17.9 eV, as the peak in the CH_2Br^-/CH_3Br spectrum (Fig. 3). What is somewhat surprising is that in all these cases, the cross section for X^- formation is much greater than for CH_2X^- formation, suggesting preferential C–X over C–H bond cleavage. Yet these ion-pair states are crossing Rydberg states converging on the $\tilde{C}\ ^2A_1$ state of CH_3X^+ where an electron has been excited from the $2a_1$ molecular orbital which has more C–H than C–X σ-character.[4–6,8] Thus excitation of this electron might be expected to weaken the C–H σ-bond to a greater extent.

The peak at *ca.* 22 eV in the CHF^-/CH_3F spectrum (Fig. 1) matches the energy of feature F3 of the F^-/CH_3F spectrum (Fig. 5), so both anions at this energy are probably formed by predissociation of the $(2a_1)^{-1}4p$ Rydberg state of CH_3F. Similarly, there is a very weak peak in the $CHBr^-/CH_3Br$ spectrum at *ca.* 18 eV (Fig. 3), but this precedes the thermochemical onset of reactions (19) and (20) and is more likely to be an artefact of CH_2Br^- detection at this energy.

5.4 Absolute cross sections for anion production from CH_3X

The absolute cross sections for anion formation from CH_3X (X = F, Cl and Br) are presented in Table 1. Those for X^- formation are slightly larger than the estimated range of 10^{-20} to 10^{-21} cm^2 quoted by Suzuki *et al.*,[10] but are a factor of *ca.* six smaller than the absolute cross sections determined by Shaw *et al.* for *total* ion-pair formation from ion detection below the ionisation threshold of the parent molecule.[2] We have noted before the difficulty of interpreting the cross sections determined in the experiments of Suzuki *et al.*, and in particular whether they have allowed for mass discrimination effects.[23] Our values should, however, be comparable with those of Shaw *et al.*, as X^- is by far the dominant anion produced in the three molecules and, based on thermochemical grounds, is the only species that can form below the first ionisation energy of each molecule. Using our cross section values together with total photoabsorption cross sections,[15–17,34] the absolute quantum yields for the peak cross section of each anion formed have been calculated (Table 1). They take values in the range $(0.4–2.3) \times 10^{-3}$ for X^- formation, and values in the range 10^{-7} to 10^{-4} for the other anions. The X^- quantum yields are quite high compared to those obtained in earlier studies of CF_3X, CH_4 and SF_5CF_3,[21–23] whereas the quantum yields for the other anions formed are of the same order of magnitude.

Table 3 Upper limits to bond dissociation energies and comparisons with literature values

Bond	D^o_{298}/eV	
	This work	Literature value[c]
H_3C-F	$\leq 5.84 \pm 0.02$[a]	4.770 ± 0.087
H_3C-Cl	$\leq 3.81 \pm 0.02$[a]	3.630 ± 0.018
H_3C-Br	$\leq 2.98 \pm 0.02$[a]	3.048 ± 0.025
FH_2C-H	$\leq 4.8_4 \pm 0.2_7$[b]	4.392 ± 0.044
ClH_2C-H	$\leq 4.3_3 \pm 0.2_6$[b]	4.343 ± 0.024
BrH_2C-H	$\leq 4.2_8 \pm 0.2_4$[b]	4.428 ± 0.025

[a] Calculated from the AE of X^- formation from CH_3X, in Fig. 4. The compound errors have contributions from the errors in AE (X^-), typically 0.02 eV, and the error in IE (CH_3), 0.01 eV. [b] Calculated from the AE of CH_2X^- formation from CH_3X, in Fig. 1–3. The errors are dominated by errors in AE (CH_2X^-), typically 0.2 eV. [c] Ref. 41.

5.5 Bond dissociation energies

Using the inequality of eqn (I), the experimental AE values for anion formation determined in this work can be used to calculate upper limits to bond dissociation energies, D^o_{298}, when the AE correlates to *single*-bond breaking ion-pair dissociation. The AE values of X^- formation presented in Table 1 and Fig. 4 are used with the IE of the CH_3 radical (9.84 ± 0.01 eV)[36] and the EA of the respective halogen atom (F (3.401 eV); Cl (3.613 eV); Br (3.364 eV))[37] for the C–X bond cleavage, and with the IE of H (13.606 eV) and the EA of the respective counter radical (CH_2F (0.25 ± 0.18 eV),[38] CH_2Cl (0.74 ± 0.16),[39] CH_2Br (0.79 ± 0.14))[40] for the C–H bond cleavage. The resulting upper limits to bond dissociation energies are presented in Table 3, and are compared to literature values.[41] An alternative way to present the data for XH_2C-H bond cleavage is to use literature values for the bond dissociation energies, and calculate a lower limit to the electron affinity of the CH_2X radical. We then obtain $EA(CH_2F) \geq -0.2_0 \pm 0.2$ eV, $EA(CH_2Cl) \geq 0.7_5 \pm 0.2$ eV, and $EA(CH_2Br) \geq 0.9_3 \pm 0.2$ eV, all consistent within error limits of literature values.[38–40]

With the possible exception of the H_3C-Br data where the values for D^o_{298} are within error limits, there is excellent consistency between the upper-limit values for $D^o_{298}(H_3C-X)$ and for $D^o_{298}(XH_2C-H)$ obtained indirectly from this ion-pair work and the accepted literature values. Furthermore, the significant difference between the upper limit for $D^o(CH_3-F)$ from this work and the literature value is in excellent agreement with the large kinetic energy of over 1 eV measured by Locht *et al.* for reaction (1) by ion kinetic energy analysis in photoionisation mass spectrometry.[42] It is also interesting to note that the upper-limit value tends toward the accurate value as the size of the halogen atom increases from F to Br. This trend has also been observed in our ion-pair work on CF_3X molecules (X = F, Cl, Br, I).[22] As the size of X increases, the density of Rydberg states increases, increasing the likelihood of a Rydberg state crossing with an ion-pair state at as low an energy as thermochemically possible, thereby reducing the inequality presented in eqn (I) ultimately to an equality.

6. Conclusions

Absolute cross sections and quantum yields for production of X^-, CH_2X^-, CHX^- and CX^- from CH_3X (X = F, Cl, Br) over the energy range 8–35 eV have been determined. The relative ion yield spectrum of H^- from CH_3Br has also been measured. The signals of all the ions display a linear dependence with pressure, showing that they arise from an ion-pair mechanism and not from the multi-step process of dissociative electron attachment. The CH_2X^-, CHX^-, CX^- and H^- spectra are observed for the first time, the X^- spectra are very similar to those reported by Suzuki *et al.*[10] The X^- cross sections are somewhat larger than the approximate range of 10^{-21} to 10^{-20} cm^2 quoted by Suzuki *et al.*, but a factor of *ca.* six smaller than the cross sections determined by Shaw *et al.* for total ion-pair formation.[2] The discrete structure in the spectra suggests that most of the anions form indirectly by predissociative crossing of an initially-excited Rydberg state of the parent molecule into an ion-pair continuum; the one exception is the lowest-energy peak of F^- from CH_3F at 13.4 eV, where its width and lack of structure suggest it may correspond to a direct ion-pair transition. The cross sections for formation of $X^- + CH_3^+$ (cleavage of the C–X bond) greatly exceed those for formation of $CH_2X^- + H^+$ (cleavage of a C–H bond), suggesting a very different coupling strength of these two ion-pair states to the molecular Rydberg states. By comparing the appearance energy of the X^-, H^-, CHX^- and CX^- anions with thermochemical thresholds, it is possible to make sensible assignments of what the partner cation (+ neutral species) are; CH_2X^- can only form with H^+. Appearance energies of X^- and CH_2X^- can be used to calculate upper limits to 298 K bond dissociation energies for $D^o(H_3C-X)$ and $D^o(XH_2C-H)$. The data are consistent with literature values.

Acknowledgements

We thank Dr David Shaw for help in running experiments on Beamline 3.1 of the Daresbury SRS, Dr Michael Parkes for help with data collection, and Dr Robert Locht (Université de Liège, Belgium) for drawing our attention to his earlier study on CH_3F. This collaboration between the groups in Birmingham and Belfast was partially funded by EPSRC Network Grant No. GR/N26234/01. The Science and Technology Facilities Council is thanked for the provision of beamtime.

References

1 J. Berkowitz, *VUV and soft X-ray photoionisation*, ed. U. Becker and D. A. Shirley, Plenum Press, New York, 1996, ch. 8.
2 D. A. Shaw, D. M. P. Holland and I. C. Walker, *J. Phys. B: At., Mol. Opt. Phys.*, 2006, **39**, 3549.
3 Intergovernmental Panel on Climate Change, United Nations, 2007, Working Group I, ch. 2.
4 L. Karlsson, R. Jadrny, L. Mattsson, F. T. Chau and K. Siegbahn, *Phys. Scr.*, 1977, **16**, 225.
5 T. N. Olney, W. F. Chan, G. Cooper, C. E. Brion and K. H. Tan, *J. Electron Spectrosc. Relat. Phenom.*, 1993, **66**, 83.
6 R. Locht, B. Leyh, D. Dehareng, K. Hottmann, H. W. Jochims and H. Baumgartel, *Chem. Phys.*, 2006, **323**, 458.
7 J. Harvey, N. J. Rogers, M. J. Simpson, R. P. Tuckett, A. Bodi, M. Johnson and T. Gerber, unpublished data.
8 M. S. Banna, B. E. Hills, D. W. Davis and D. A. Shirley, *J. Chem. Phys.*, 1974, **61**, 4780.
9 M. S. Banna and D. A. Shirley, *Chem. Phys. Lett.*, 1975, **33**, 441.
10 S. Suzuki, K. Mitsuke, T. Imamura and I. Koyano, *J. Chem. Phys.*, 1992, **96**, 7500.

11 K. Suto, Y. Sato, C. L. Reed, V. Skorokhodov, Y. Matsumi and M. Kawasaki, *J. Phys. Chem. A*, 1997, **101**, 1222.
12 D. D. Xu, J. Huang, R. J. Price and W. M. Jackson, *J. Phys. Chem. A*, 2004, **108**, 9916.
13 A. G. Suits and J. W. Hepburn, *Annu. Rev. Phys. Chem.*, 2006, **57**, 431.
14 W. Li, R. R. Lucchese, A. Doyuran, Z. Wu, H. Loos, G. E. Hall and A. G. Suits, *Phys. Rev. Lett.*, 2004, **92**, 1.
15 R. Locht, B. Leyh, A. Hoxha, D. Dehareng, H. W. Jochims and H. Baumgärtel, *Chem. Phys.*, 2000, **257**, 283.
16 R. Locht, B. Leyh, A. Hoxha, D. Dehareng, K. Hottmann, H. W. Jochims and H. Baumgärtel, *Chem. Phys.*, 2001, **272**, 259.
17 R. Locht, B. Leyh, H. W. Jochims and H. Baumgärtel, *Chem. Phys.*, 2005, **317**, 73.
18 C. A. Hunniford, S. W. J. Scully, K. F. Dunn and C. J. Latimer, *J. Phys. B: At., Mol. Opt. Phys.*, 2007, **40**, 1225.
19 C. R. Howle, S. Ali, R. P. Tuckett, D. A. Shaw and J. B. West, *Nucl. Instrum. Methods Phys. Res., Sect. B*, 2005, **237**, 656.
20 K. F. Dunn, 2009, private communication.
21 M. J. Simpson, R. P. Tuckett, K. F. Dunn, C. A. Hunniford, C. J. Latimer and S. W. J. Scully, *J. Chem. Phys.*, 2008, **128**, 124315.
22 M. J. Simpson, R. P. Tuckett, K. F. Dunn, C. A. Hunniford and C. J. Latimer, *J. Chem. Phys.*, 2009, **130**, 194302.
23 N. J. Rogers, M. J. Simpson, R. P. Tuckett, K. F. Dunn and C. J. Latimer, *Mol. Phys.*, 2010, **108**, 895.
24 P. H. Dawson, *Quadrupole Mass Spectrometry and its Applications*, American Vacuum Society Classics, American Institute of Physics, New York, 1995.
25 K. Mitsuke, S. Suzuki, T. Imamura and I. Koyano, *J. Chem. Phys.*, 1990, **93**, 8717.
26 K. Mitsuke, S. Suzuki, T. Imamura and I. Koyano, *J. Chem. Phys.*, 1991, **95**, 2398.
27 P. M. Dehmer and W. A. Chupka, *J. Chem. Phys.*, 1975, **62**, 4525.
28 J. C. Traeger and R. G. McLoughlin, *J. Am. Chem. Soc.*, 1981, **103**, 3647.
29 M. W. Chase, *J. Phys. Chem. Ref. Data Monogr.*, 1998, **9**, 1.
30 S. G. Lias, J. E. Bartmess, J. F. Liebman, J. L. Holmes, R. D. Levin and W. G. Mallard, *J. Phys. Chem. Ref. Data*, 1988, **17**, 1.
31 R. Locht, B. Leyh, A. Hoxha, D. Dehareng, K. Hottmann, H. W. Jochims and H. Baumgartel, *Chem. Phys.*, 2001, **272**, 293.
32 A. P. Hitchcock and C. E. Brion, *J. Electron Spectrosc. Relat. Phenom.*, 1978, **13**, 193.
33 C. A. Theodosiou, M. Inokuti and S. T. Manson, *At. Data Nucl. Data Tables*, 1986, **35**, 473.
34 C. Y. R. Wu, L. C. Lee and D. L. Judge, *J. Chem. Phys.*, 1979, **71**, 5221.
35 H. Yoshida and K. Mitsuke, *J. Electron Spectrosc. Relat. Phenom.*, 1996, **79**, 487.
36 A. M. Schulenburg, C. Alcaraz, G. Grassi and F. Merkt, *J. Chem. Phys.*, 2006, **125**, 104310.
37 J. C. Rienstra-Kiracofe, G. S. Tschumper, H. F. Schaeffer, S. Nandi and G. B. Ellison, *Chem. Rev.*, 2002, **102**, 231.
38 S. T. Graul and R. R. Squires, *J. Am. Chem. Soc.*, 1990, **112**, 2517.
39 S. Ingemann and N. M. M. Nibbering, *J. Chem. Soc., Perkin Trans. 2*, 1985, 837.
40 P. M. Hierl, M. J. Henchman and J. F. Paulson, *Int. J. Mass Spectrom. Ion Processes*, 1992, **117**, 475.
41 *CRC Handbook of Chemistry and Physics*, ed. D. R. Lide, Taylor and Francis, London, 90th edn, 2009.
42 R. Locht, J. Momigny, E. Rühl and H. Baumgärtel, *Chem. Phys.*, 1987, **117**, 305.

